

Crop lodging induced by wind and rain

Martinez-Vazquez, Pedro

DOI:

[10.1016/j.agrformet.2016.07.003](https://doi.org/10.1016/j.agrformet.2016.07.003)

License:

Creative Commons: Attribution-NonCommercial-NoDerivs (CC BY-NC-ND)

Document Version

Peer reviewed version

Citation for published version (Harvard):

Martinez-Vazquez, P 2016, 'Crop lodging induced by wind and rain', *Agricultural and Forest Meteorology*, vol. 228-229, pp. 265-275. <https://doi.org/10.1016/j.agrformet.2016.07.003>

[Link to publication on Research at Birmingham portal](#)

Publisher Rights Statement:

Checked 15/7/2016

General rights

Unless a licence is specified above, all rights (including copyright and moral rights) in this document are retained by the authors and/or the copyright holders. The express permission of the copyright holder must be obtained for any use of this material other than for purposes permitted by law.

- Users may freely distribute the URL that is used to identify this publication.
- Users may download and/or print one copy of the publication from the University of Birmingham research portal for the purpose of private study or non-commercial research.
- User may use extracts from the document in line with the concept of 'fair dealing' under the Copyright, Designs and Patents Act 1988 (?)
- Users may not further distribute the material nor use it for the purposes of commercial gain.

Where a licence is displayed above, please note the terms and conditions of the licence govern your use of this document.

When citing, please reference the published version.

Take down policy

While the University of Birmingham exercises care and attention in making items available there are rare occasions when an item has been uploaded in error or has been deemed to be commercially or otherwise sensitive.

If you believe that this is the case for this document, please contact UBIRA@lists.bham.ac.uk providing details and we will remove access to the work immediately and investigate.

Crop lodging induced by wind and rain

P. Martinez-Vazquez

School of Civil Engineering, University of Birmingham B15 2TT, UK
Tel. 0121 414 5059; Email: p.vazquez@bham.ac.uk

Abstract

A methodology to estimate wind and rain effects on the four main growth crops in the United Kingdom is presented. The method is based on simulated weather scenarios acting on synthetic plants over a period of thirty years. The environmental data is generated with the UKCP09 Weather Generator considering future climate scenarios whereas plants are modelled as simple oscillators characterised by their mass, stiffness and damping. The joint probability of occurrence of wind and rain are estimated together with the conditions in which lodging would occur. The paper shows that the dynamic response of plants varies with season being the three months of the year the most critical whilst the plants' performances define crop failure velocities ranging between 4 ms^{-1} and 23 ms^{-1} and associated failure rates of 50% and 5% per unitary velocity.

Key works: crop lodging; wind simulation; environmental modelling; UKCP09 Weather Generator

1. Introduction

The interaction of plants with the wind and the nature of plant failures which can occur during periods of high winds have been much investigated in the past. In Wright (1965) it was noticed that the characteristics of the flow through a canopy varied within the crop height and hence some parameterisation of the observed variation was proposed. Baines (1971), Denmead and Bradley (1967), Finnigan and Mulhearn (1968), and Cionco (1972) also discussed the nature of turbulence within canopies and provided additional insight of the flow dynamics that govern the energy flow exchange in canopies. A review of the interaction of plants with the wind can also be found in de Langre (2008). In terms of plant's modelling, Sellier et al (2006) investigate the oscillation of trees via numerical modelling whilst Rodriguez et al (2009) carried out experimental work to determine natural frequencies of walnut trees. For isolated plants the work of Baker (Baker, 1995; Baker et al., 1998; Sterling et al (2003); Berry et al 2003; Saunderson et al (1999; 2000) is notable. Baker (1995) assumed that wheat plants and isolated trees could be idealised as two simple masses connected by a light inextensible element. The first mass represented the root-soil structure of the plant while the

32 second represented the mass of the plant. Baker's model enabled the maximum wind induced base
33 bending moment to be obtained which seemed reasonable when compared to the natural variations
34 which can occur in the plant properties (e.g. stem diameter, root plate spread etc.). More recently,
35 Martinez-Vazquez and Sterling (2011) showed that the model proposed in Baker (1995) can in fact be
36 used to calculate lodging for large populations of plants. The present investigation builds on previous
37 research and attempts to merge mechanical modelling techniques for plants with statistical predictions
38 of environmental variables to calculate crop's behaviour. Environmental variables are simulated by
39 the UKCP09 Weather Generator. This is a facility that enables constructing future climate scenarios
40 from where rain and wind conditions can be determined. In this investigation wind and rain scenarios
41 are used to test plant crops in order to observe conditions that induce their failure. Four types of plants
42 are considered, these are oats, wheat, barley, and rapeseed. The similarities and differences amongst
43 the various plant responses are compared and discussed throughout.

44 The paper is organised as follows. Section 2 outlines the characteristics of the weather generator and
45 its prediction capabilities; section 3 provides the details of how to generate wind and rain databases
46 based on the prediction tool; section 4 describes how the wind turbulence within a canopy was
47 modelled; section 5 details the generation of synthetic plants, taking oats as a case study; section 6
48 explains how to estimate the plant's resistance for the use of Baker's simplified model; section 7 give
49 full results of the response of oat crops subject to wind and rain; section 8 extends the plant response
50 analysis to the other plant types, whilst section 9 provides some final remarks.

51 **2. The UKCP09 Weather Generator**

52 In recent years the Met Office Hadley Centre in collaboration with UK Climate impacts Programme
53 and over thirty other organisations have developed the UKCP09 Weather Generator aiming at
54 visualising future climate fluctuations across the United Kingdom. This facility is capable to provide
55 weather scenarios and associated measures of uncertainty until 2080. In the present research this tool
56 was used to determine the most probable combinations of wind and rain that are likely to occur on the
57 region of Cardington, UK (52.1055 °N, 0.4244 °W 29 m above MSL) and to evaluate their combined
58 effect on oat crops.

59 The UKCP09 user's interface provides access to customised outputs that reflect the underlying
60 UKCP09 climate projections. Pre-prepared maps and graphs can be used to select any land or marine
61 region – defined by 5 km², within the UK. The available data includes 17 variables over land areas
62 and 4 over marine regions. The following are the weather parameters over land areas that can be
63 generated by using the referred tool (Jenkins et al, 2009).

- 64 ▪ Mean temperature (°C)
- 65 ▪ Mean daily maximum temperature (°C)
- 66 ▪ Mean daily minimum temperature (°C)
- 67 ▪ 99th percentile of daily maximum temperature in a season (warmest day of the season) (°C)
- 68 ▪ 1st percentile of daily maximum temperature in a season (coolest day of the season) (°C)
- 69 ▪ 99th percentile of daily minimum temperature in a season (warmest night of the season) (°C)
- 70 ▪ 1st percentile of daily minimum temperature in a season (coldest day of the season) (°C)
- 71 ▪ Precipitation rate (mm/day)
- 72 ▪ 99th percentile of daily precipitation rate in the season (wettest day of the season) (mm/day)
- 73 ▪ Specific humidity (%)
- 74 ▪ Relative humidity (%)
- 75 ▪ Total cloud (%)
- 76 ▪ Net surface long wave flux (W/m²)
- 77 ▪ Net surface short wave flux (W/m²)
- 78 ▪ Total downward short wave flux (W/m²)
- 79 ▪ Mean sea level pressure (hPa)
- 80 ▪ Grass reference evapotranspiration (mm/day)

81

82 Environmental data for any selected region are accessed by setting up a request to the UKCP09
83 central unit for instance by following the procedure given in Appendix A. After the request is made
84 the simulated data is made available to download.

85

86 3. Hourly rain and wind database

87 The amount of rain per day and per hour is directly available from the output of the UKCP09
88 simulator but not for the velocity of the wind. In such case one can estimate the hourly wind regime
89 through a two-step process namely (i) inferring the daily winds by using the grass reference
90 evapotranspiration parameter (only available on a daily basis) and (ii) downscaling the data to
91 estimate hourly winds. The way this process was applied for this research is described in the
92 following paragraphs.

93 3.1 Daily wind

94 There are a number of methods to infer the wind from the environmental parameters such as those
95 discussed in Ventura (1999), Allen (1994), Ekström et al (2007), and Eames et al (2011), to mention
96 some. These approaches are based on the reference evapotranspiration ET_0 which is calibrated based
97 on full-scale observations. In this research the 24-h FAO Penman-Monteith equation - as described in
98 Ventura (1999), was used. This approximation is given by Eq. (1) below.

99

$$100 \quad PET = \frac{0.408\Delta(R_n - G) + \gamma \frac{900}{T + 273.16} U_2 (e_a - e_d)}{\Delta + \gamma(1 + 0.34U_2)} \quad (1)$$

101 PET : grass reference evapotranspiration (mm day^{-1})

102 R_n : net radiation at crop surface ($\text{MJ m}^{-2} \text{day}^{-1}$)

103 G : soil heat flux ($\text{MJ m}^{-2} \text{day}^{-1}$) – assumed to be zero as in Ekström et al (2007)

104 T : mean temperature at 2 m height ($^{\circ}\text{C}$)

105 U_2 : wind speed measured at 2 m height (m s^{-1})

106 $(e_a - e_d)$: vapour pressure deficit for measurement at 2 m height (kPa)

107 Δ : slope of the vapour pressure curve ($\text{kPa } ^{\circ}\text{C}^{-1}$)

108 γ : psychrometric constant ($\text{kPa } ^{\circ}\text{C}^{-1}$)

109 900 : coefficient for the reference crop ($\text{kJ}^{-1} \text{kg K day}^{-1}$) – see Allen et al (1994)

110 0.34 : wind coefficient for the reference crop (s m^{-1})

111 Eq. (1) can be re-arranged as in Eq. (2a) in order to infer daily mean velocities of wind.

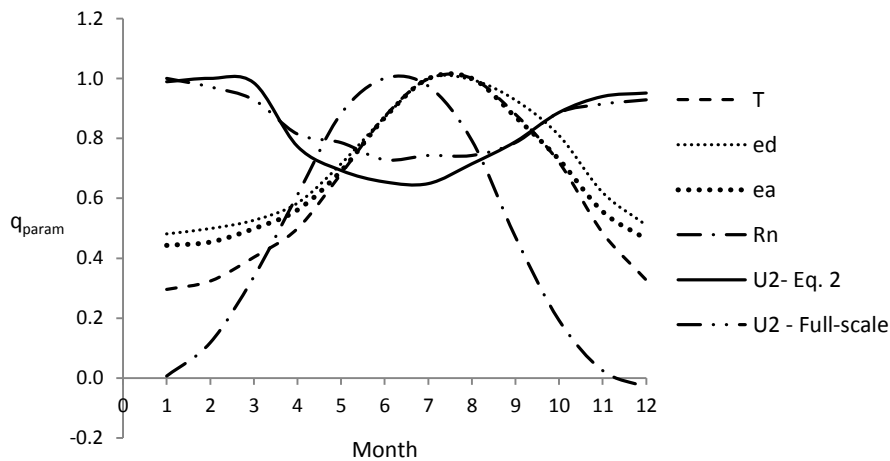
112
$$U_2 = \frac{PET(\Delta+\gamma)-X}{(YZ-0.34\gamma PET)} \quad (2a)$$

113 where

114
$$X = 0.408\Delta(R_n - G); Y = \gamma \frac{900}{T+273.16}; Z = e_a - e_d \quad (2b)$$

115 The equations to calculate all parameters for estimating U_2 in Eq. (2a) are given in Appendix B.

116 The data provided by the weather generator was passed through Eq. (2) and then averaged per month
 117 in order to establish a comparison with full-scale statistics issued by in Met office (2013) – in terms of
 118 wind velocity. The results of the data processing for hundred scenarios of 30-years each are presented
 119 in normalised form in Fig. 1 whilst Table 1 provides the peak values of each environmental
 120 parameter. Note that full-scale measurements have been normalised by the peak simulated value in
 121 order to show the actual relationship between the two vectors.



122
 123
 124 Fig. 1 Monthly average of environmental parameters related to PET .
 125
 126

127 Table 1. Peak values of environmental parameters (q_{param}) related to the reference evapotranspiration

T ($^{\circ}C$)	e_d kPa	e_a kPa	R_n $MJm^{-2}day^{-1}$	U_2 (ms^{-1}) Eq. 2	U_2 (ms^{-1}) Full-scale
18.04	1.52	2.01	11.56	3.85	3.5

128

129 In Fig. 1 is seen that the net radiation profile (R_n) is out of phase with respect to temperature (T) which
 130 might be due to the influenced of solar declination and relative distance with respect to the sun.

131 Actual (e_a) and saturated (e_s) vapour pressure seem strongly correlated to T whilst the peak wind
 132 velocity occurs near the equinoxes, which is consistent with full-scale observations. The average ratio
 133 full-scale to simulated wind data is of 1.045. Thus according to the UKCP09 future scenarios, wind
 134 velocity will increase or decrease at a rate of about 4.5% within a horizon of 30 years (Jenkins et al
 135 2009).

136 Full-scale data was inferred from the Virtual Met Mast Report (Met office 2013) which is located in
 137 Cardington, UK. For that report measurements were taken at a height of 50 m thus for the purpose of
 138 comparison the data was scaled to 2 m above the ground by using the relationship $U_z = (z/z_r)^Y$ with z_r
 139 = 10 m and $Y = 0.22$. The inferred average and peak reference values used here are provided in Table
 140 2.

141 Table 2. Peak and average values of U_2 as inferred from Met Office (2013)

Month	1	2	3	4	5	6	7	8	9	10	11	12
$U_{2,peak}$	15.2	15	14	12.4	12	11.3	11	11.2	12	12.5	13.7	14.5
$U_{2,mean}$	7	6.8	6.5	5.7	5.5	5.1	5.2	5.2	5.2	6.2	6.5	6.5

142

143 3.2 Hourly wind

144 The average hourly winds registered at Cardington (Met office, 2013) exhibit day fluctuations that can
 145 be approximated by Eq. (3) - where \hat{U} represents hourly velocity normalised by the mean value. U_{24}
 146 and t , are the velocity at 24-hrs and time of the day (hr) respectively.

$$147 \hat{U} = A \left[-\sin \left(\frac{\pi(t-F)}{Fx} \right) \right] + \frac{t(t-E)}{BC} + D \cdot U_{24} \quad (3)$$

148 with $A = 0.16$; $B = 60$; $C = 22$; $D = 1.13$; $E = 31$; $F = 22$; $x = 0.63$

149 The estimated mean square error between the proposed Eq. (3) and full-scale measurements was of
 150 about 1.11%. This approximation was used to infer hourly winds from daily records followed by
 151 monthly probability distributions. The latter are shown in Fig. 2a whereas Fig. 2b shows average
 152 probability distributions calculated per period of three months. Similarly future scenarios provided by
 153 the UKCP09 Weather Generator were used to calculate the probability distribution of daily rain which
 154 is shown in Fig. 3.

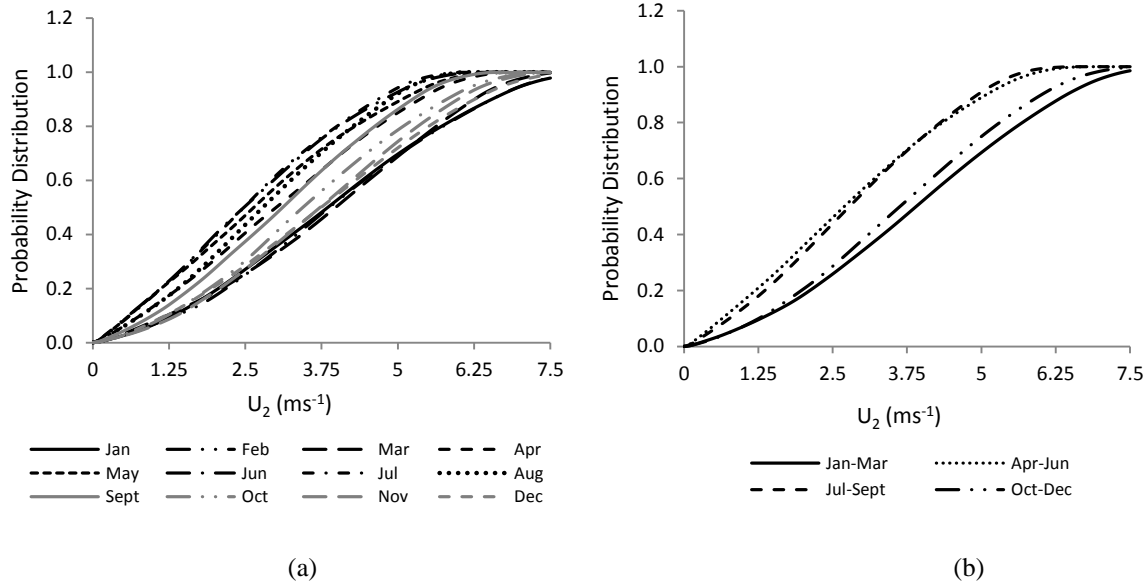


Fig. 2 Probability distribution for wind (a) per month and (b) three-month average.

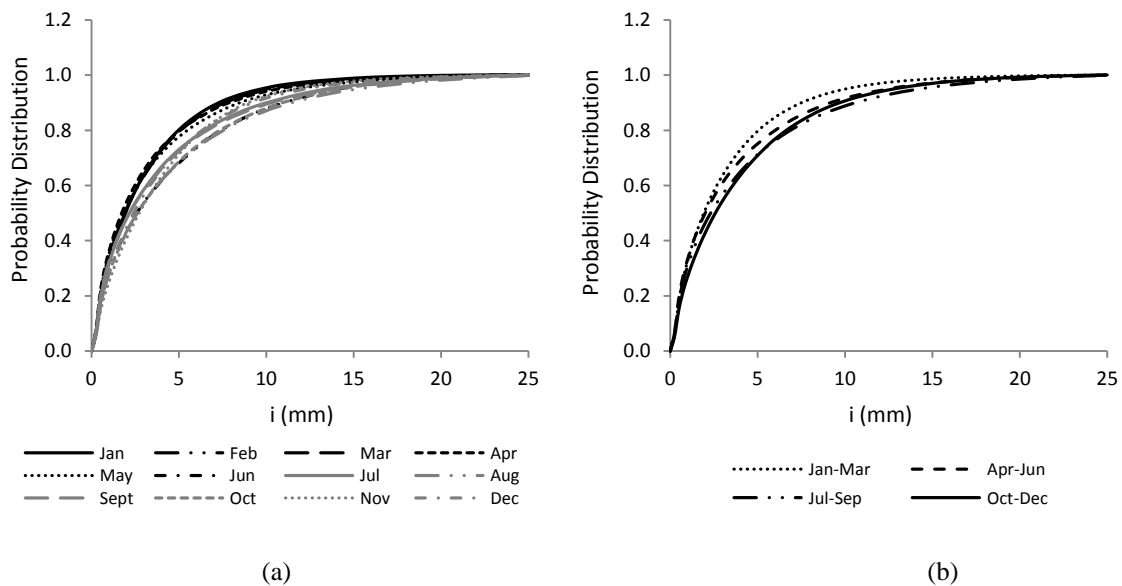


Fig. 3 Probability distribution for rain (a) per month and (b) three-month average.

155
156
157
158
159
160

161
162
163
164

165
166

167 In Fig. 2a the change of maximum wind speed over the year has been reflected. The wind velocity
168 tends to be lower during summer and therefore their probability distribution $P [q \leq U_2]$ - where q is
169 the instantaneous velocity at 2 m above the ground, exhibits higher rates of change in comparison
170 with winter times. This can be more clearly appreciated in Fig. 2b where three-month averages have
171 been represented. In the case of rain the records show an increase towards the end of the year with

172 less variation during the first six months. Three-month averages suggest that the amount of daily rain
 173 is fairly uniform during the year. However note that the probability distribution shown in Fig. 3 does
 174 not reflect the probability of precipitation but the level of rain when it does occur. The former i.e. $P[i$
 175 $> 0]$, was estimated separately and is provided in Table 3. Fig. 3 also predicts that within a horizon of
 176 30 years the amount of rain that will be exceeded 50% of the time ranges between 1.75 (Apr) and 2.75
 177 (Nov) mm which is consistent with the expected value of 2 mm that has characterised the UK - see
 178 Baker (1998).

179 The probabilistic analysis was completed by defining Weibull distribution curves to characterise
 180 hourly winds and accumulated rain per month. Eq. (4) gives the general form of the Weibull function
 181 whilst Table 3 shows the shape (ϑ) and scale parameters (α) that resulted from the analysis. Note that
 182 the variable x in Eq. (4) represents wind or rain.

$$183 \quad (v) = \frac{\vartheta}{\alpha} \left(\frac{x}{\alpha}\right)^{\vartheta-1} e^{-(x/\alpha)^\vartheta} \quad (4)$$

184 Table 3. Weibull parameters that represent probability density functions for wind and rain

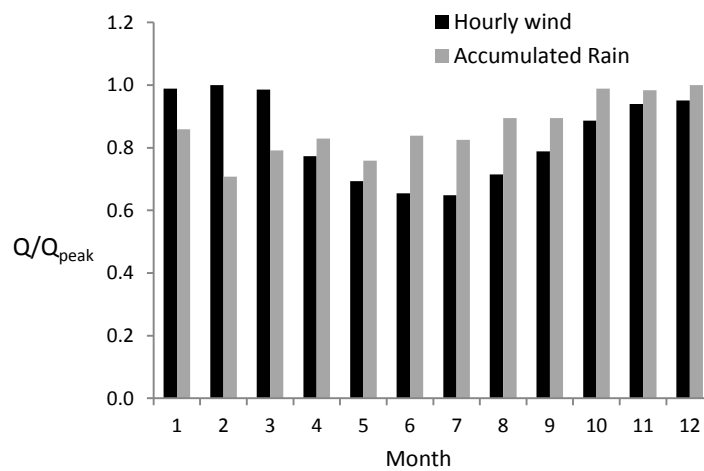
Month	Wind (U_2)		Rain (i)		$P[i > 0]$
	ϑ	α	ϑ	α	
1	2.2	4.8	0.76	2.6	0.497
2	2.2	4.8	0.76	2.4	0.439
3	2.1	4.7	0.76	2.4	0.451
4	1.82	3.8	0.80	2.0	0.472
5	1.53	3.3	0.85	1.8	0.388
6	1.67	3.3	0.70	2.9	0.335
7	1.74	3.3	0.70	2.6	0.347
8	1.95	3.8	0.75	3.1	0.314
9	2.0	4.0	0.75	2.8	0.378
10	2.0	4.1	0.75	3.4	0.379
11	2.3	4.6	0.80	3.9	0.459
12	2.0	4.6	0.75	3.3	0.460

185

186 The value of shape factors shown in Table 3 indicate that rain is a highly skewed process resembling
 187 an exponential form whilst hourly wind is asymmetric with respect to the mean value. The average

188 shape factor predicted by the UKCP09 Weather generator across the year is of 1.96. The Met Office
 189 (2013) reports a shape factor of 2.16 for historical data referred to 50 m above the ground level.
 190 However these measurements correspond to different heights the increase of skewness of pdfs as the
 191 locations approaches to the ground seems reasonable.

192 Finally, Fig. 4 shows an overview of the variability of hourly wind and accumulated rain over the year
 193 in normalised form. In this figure the peak value of wind is of 3.85 – see table 1, whereas the peak
 194 value of accumulated rain during the month is of 54.4 mm.



195
 196 Fig. 4. Variation of hourly wind and accumulated rain across a year (30-year horizon).

197

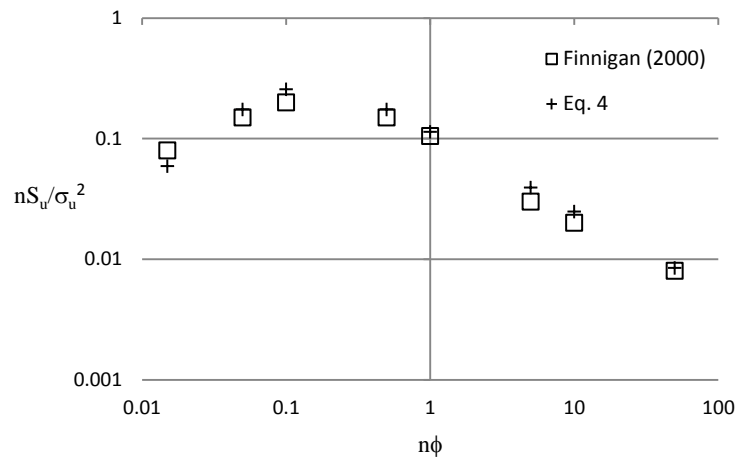
198 **4. Wind turbulence within the canopy**

199 Finnigan (2000) has shown that turbulence within plant canopies differs from that of the surface layer.
 200 This variation is due energy short-cutting of the spectral cascade due to vortex shedding on the plants
 201 (larger eddies broken up into smaller eddies very rapidly). Thus the energy loss that occurs inside the
 202 canopy should be considered when estimating wind effects on cereal crops. Finnigan (2000) presents
 203 the variation of the spectral density $nS_u(n)/\sigma^2$ with $n\phi$ where $\phi = h_c/U(h_c)$ – being $U(h_c)$ and
 204 h_c the average mean velocity inside the canopy and the height of the crop respectively. Although no
 205 equation to generate the continuous spectral density is provided by Finnigan (2000) it has been
 206 observed in this study that the shape of the spectrum is similar inside and outside the canopy. This is
 207 demonstrated in Fig. 5 which compares a scaled version of the Von Karman’s wind power spectrum –

208 given by Eq. (5), with the results presented by Finnigan (2000). In Eq. (5) the reduced frequency $n\phi$
 209 is taken as independent variable as in Finnigan (2000). It follows that a suitable scaled version of the
 210 standard wind power spectrum can be used to represent turbulence inside the canopy. The
 211 recommended spectrum to represent turbulence inside the canopy is thus given by Eq. (5).

$$212 \quad \frac{nS_u(n)}{\sigma^2} = \frac{4(n\phi)}{(1+70.8(n\phi)^2)^{5/6}} \quad (5)$$

213



214
215

216 Fig. 5 Spectral representation of turbulence inside plant canopies.

217

218 The estimated mean square error between Eq. (5) and the spectrum presented by Finnigan (200) is of
 219 6.6 % whereas in the region $0.1 \leq n\phi \leq 100$ one obtains a mean square error of about 0.09 %. The
 220 relevance of the spectral region above 0.1 Hz is that it covers any natural period of a cereal plant that
 221 is below 10 s which is presumably 100% of the crop. Based on this results it has been decided to use
 222 Eq. (5) to represent wind turbulence within plant canopies.

223 5. Plant database

224 Berry et al (2003) have parameterised wheat plants by using data collected across 32 crops in the UK.
 225 In that study partial correlation amongst some of the plant parameters have also been established. The
 226 parameters used by Berry et al (2003) to characterised wheat are:

- 227 ▪ Centre of gravity (X) : mm

251 numbers to be projected on the cumulative distribution function of uncorrelated plant parameters to
 252 find values of the plant parameters. The plant database generated in this way is presented in Table 5.

253 Table 5. 20-Plant database

<i>Plant</i>	<i>X</i>	<i>A</i>	<i>d</i>	<i>n</i>	<i>h</i>	<i>D</i>	<i>t</i>	<i>R</i>	<i>N</i>
1	789.33	5015.79	6.44	1.5	66.34	54.86	1.24	33.36	2.18
2	973.68	4891.84	7.87	1.24	95.4	43.69	0.39	24.82	2.78
3	1150.08	4523.18	5.94	1.21	59.38	43.95	0.92	30.8	2.28
4	988.83	4838.33	6.11	1.7	49.19	57.55	1.12	29.79	2.4
5	1131.78	5031.35	5.79	1.64	46.12	39.72	1.19	27.71	2.59
6	790.23	4561.14	5.96	1.73	67.69	45.65	1.07	25.69	2.28
7	979.68	5232.15	6	1.71	75.23	46.76	1	23.88	2.6
8	1110.18	4524.55	6.73	1.19	49.79	65.22	1.2	29.99	1.98
9	920.28	5412.38	7.69	1.45	70.77	52.6	1.01	22.14	2.95
10	964.53	3737.81	7.08	1.44	70.79	59.78	0.79	36.69	1.75
11	973.68	4857.08	7.35	1.19	61.07	53.06	0.78	33.3	2.32
12	892.83	4055.72	7.92	1.72	75.06	42.78	0.86	26.84	2.97
13	903.03	4965.48	7.83	1.21	50.13	63.44	1.07	32.83	1.82
14	801.94	4642.1	5.41	1.58	55.25	50.4	1.04	28.41	2.51
15	848.58	4700.65	6.4	1.4	68.19	58.8	0.86	30.93	2.69
16	1027.68	5035.46	4.46	1.59	74.88	51.39	0.98	22.11	2.41
17	953.88	4030.1	5.66	1.35	72.59	61.59	0.89	20.23	2.08
18	1116.93	4648.96	6.11	1.32	70.69	40.4	0.8	30.89	2.95
19	756.33	4371.78	5.84	1.47	72.47	46.95	0.89	22.87	2.88
20	896.28	4770.63	6.78	1.33	74.52	60.99	1.02	22.82	3.24
mean	948.49	4692.32	6.47	1.45	66.28	51.98	0.96	27.81	2.48
stdev	118.46	413.73	0.93	0.19	11.96	8.03	0.19	4.61	0.41

254

255 6. Plant resistance

256 Plant failure can occur by root or stem insufficient resistance. The former is a function of soil
 257 moisture and extent of the root whereas the latter depends on mechanical properties and geometry of
 258 the stem. Baker (1998) provides the equations that allow the bending capacity of the root (M_r) and
 259 stem (M_s) to be estimated. For the benefit of the reader those equations are reproduced here in Eq. (7)
 260 and (8).

$$261 \quad s_w = 1484e^{-5f/c}(2.2 - 0.24v)(4.82c - 0.30) \quad (7a)$$

$$262 \quad s_d = 1125e^{-5w/c}(2.2 - 0.24v)(4.82c - 0.30) \quad (7b)$$

263 $s = s_d - \frac{i}{\rho_s/\rho_w(f-w)h} (s_d - s_w) \geq s_w$ (7c)

264 $M_r = k_s s D^3$ (7d)

265 The stem failure moment is given by,

266 $M_s = \frac{\sigma \pi d^3}{32} \left(1 - \left(\frac{d/2-t}{d/2} \right)^4 \right)$ (8)

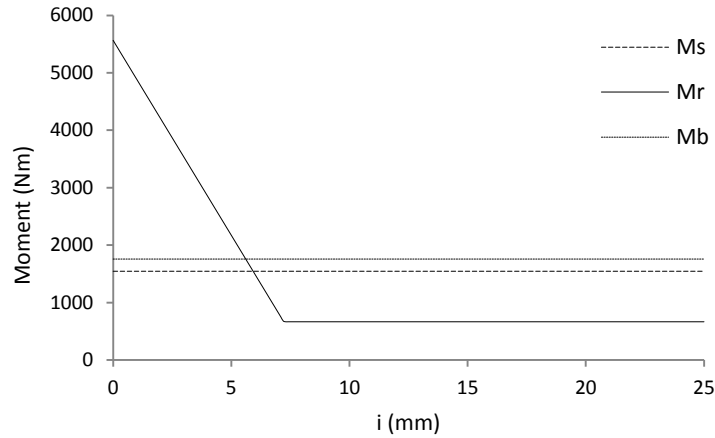
267 In these equations s_w , s_d are the shear strength for wet and dry soil conditions respectively, ρ_s and, ρ_w
 268 represent soil and water density, i is the daily rainfall that is exceeded 50% of the time, c is the clay
 269 content, v is a visual score measuring soil compaction, w is the water content at wilting point and f
 270 represents the water content at field capacity. The values for these parameters used in this study are
 271 provided in Table 6.

272 Table 6. Soil parameters

k_s	i	c	v	w	f
0.43	2.0	0.25	5	0.15	0.27

273

274 Based on Eq. (7)-(8), and using the parameters listed in Tables 5 and 6 a typical relationship between
 275 M_r , M_s , and the bending moment induced by wind (M_b) could be defined. Note that M_b is simply the
 276 result of multiplying the wind force $F_w = 1/2 \rho_{air} C_D U_2^2 A$ by the corresponding distance X – where
 277 C_D and A are the drag coefficient and area exposed to wind respectively – see Table 5. Fig. 6 shows
 278 values of M_s , M_r and M_b calculated for plant 13 and for different levels of rain (i).



279

280 Fig. 6 Typical relationship between stem and root resistance with wind-induced bending acting - oat plant 13.

281

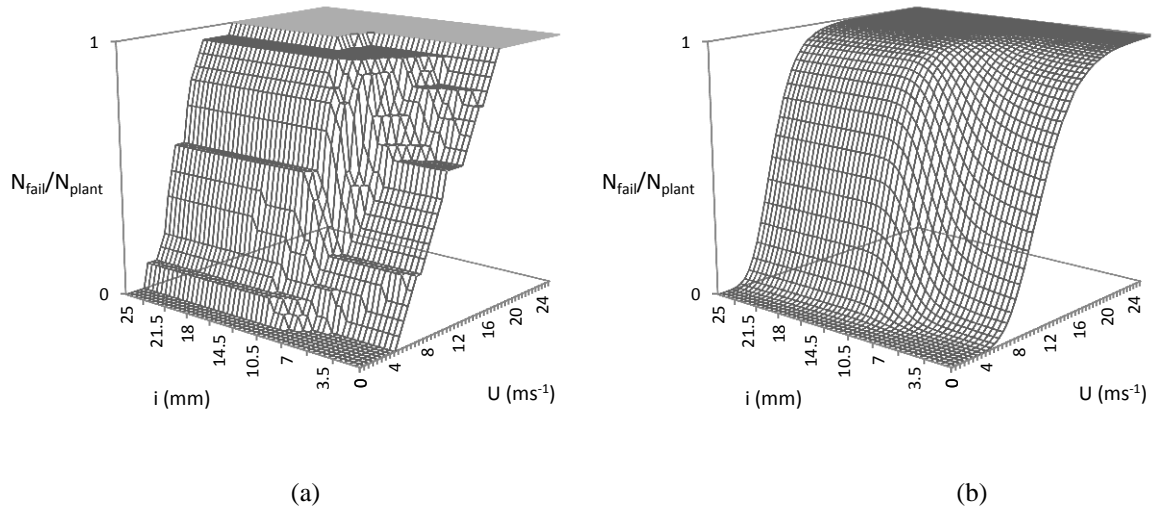
282 In Fig. 6 two regions that characterise crop failure can be identified. The first one controlled by stem
 283 resistance which according to the simulated database covers the lower precipitation range i.e. $0 \leq i <$
 284 $5-10$ (mm) whereas the second region of failure corresponds to precipitation rates above $5-10$ (mm)
 285 leading to root failure. According to Eq. 7c the root capacity is bounded by the soil shear strength at
 286 wet condition. This is consistent with Baker (1998) where Eq. 7c is validated for the interval $0 \leq i \leq$
 287 $h(f-w)\rho_s/\rho_w$ which for the average soil parameters and plant characteristics presented above translate
 288 into an upper limit of ~ 7.15 mm. In the following the lower shear strength of the soil will be
 289 considered to be constant across high rain conditions i.e. $h(f-w)\rho_s/\rho_w \leq i \leq 25$ mm in order to observe
 290 the crop behaviour under high winds however keeping in mind the identified boundary conditions.

291 7. Analysis of plant's response

292 The force induced to the plants by wind were estimated and their demand of resistance was compared
 293 against the capacity to resist the overturning moments provided by the root and the stem. This was
 294 done for a range of wind and rain levels so that the number of plants that failed could be quantified.
 295 Fig. 7a shows the quantification of failure in terms of the index N_{fail}/N_{plant} for the 20-plant database
 296 presented in Table 5 – where N_{fail} and N_{plant} are number of failed plants and number of plants in the
 297 original database respectively. Fig. 7b shows the quantification of failure for an extended database

298 including 10 000 plants. Note that the extended database was formed by using the methodology
 299 described in section 5 for the 20-plant sample.

300



301

302

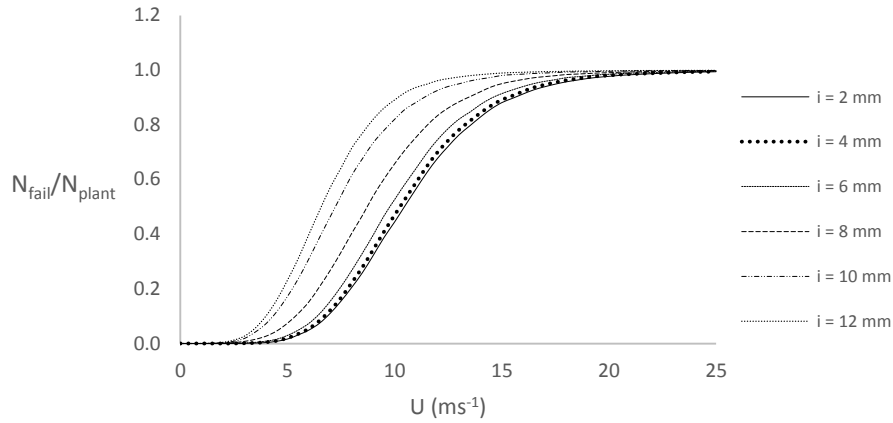
303

304 Fig. 7 Representation of Failure for the oat crop based on (a) 20-plant database and (b) 10 000 plant sample.

305

306 In Fig. 7 the two regions of failure identified in Fig. 6 have been reflected. The first region being
 307 determined by stem failure occurring for rain levels of $0 \leq i \leq h(f-w)\rho_s/\rho_w$ and characterised by a
 308 constant value of the index N_{fail}/N_{plant} with respect to i – more clearly appreciated on Fig. 7a where $h(f-$
 309 $w)\rho_s/\rho_w$ fluctuates around 7.15 mm. For levels of rain that exceed $i = h(f-w)\rho_s/\rho_w$ there is a bi-linear
 310 type of behaviour as i varies, which is predicted by Eq. (7) and (8) and illustrated in Fig. 6.

311 In order to better visualise the lodging for the domain $\{U, i\}$ presented in Fig. 7b, a range of curves
 312 representing plant failure for various levels of i are represented in Fig. 8.



313

314

Fig. 8 Index of Failure for the 10 000 plant sample for different levels of rain.

315

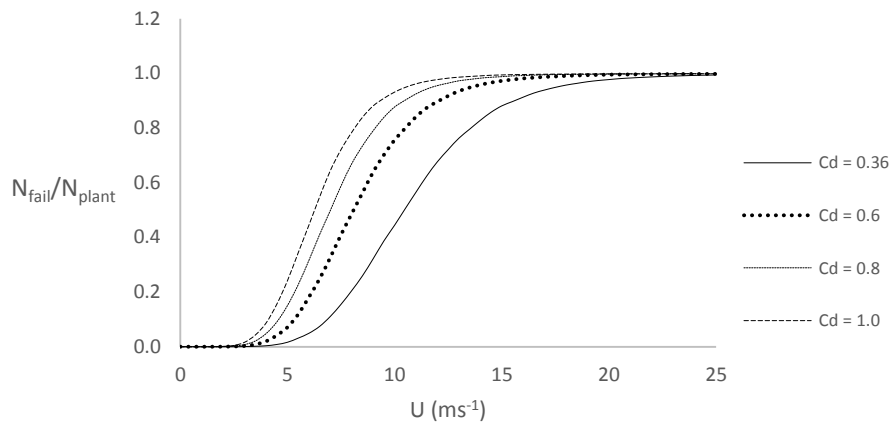
The shape of the curves in Fig. 8 is consistent with the Weibull distribution function for wind velocity (U) whose parameters are given in Table 3. It can be seen in this figure that the rate of failure increases with the level of rain. However note that no significant variation was observed for levels of rain above 12 mm - which can also be seen in Fig. 7b, and therefore the curve shown in Fig. 8 for $i = 12$ mm can be considered constant for higher levels of rain.

319

320

On the other hand, given the limited amount of experimental work undertaken as to determine the drag coefficient on oat plants (Verissimo, 2015), a parametric analysis was undertaken to investigate the percentage of plants' failure for different values of Cd and for a rain level of 2 mm. The results of this is shown in Fig. 9 for values of Cd equal to 0.36, 0.6, 0.8, and 1.0. Note that the results shown in Fig. 6-8 were estimated by considering Cd of 0.36 i.e. the lower value in the range.

324



325

326

Fig. 9 Index of Failure for the 10 000 plant sample for $i = 2$ mm and different values of Cd .

327

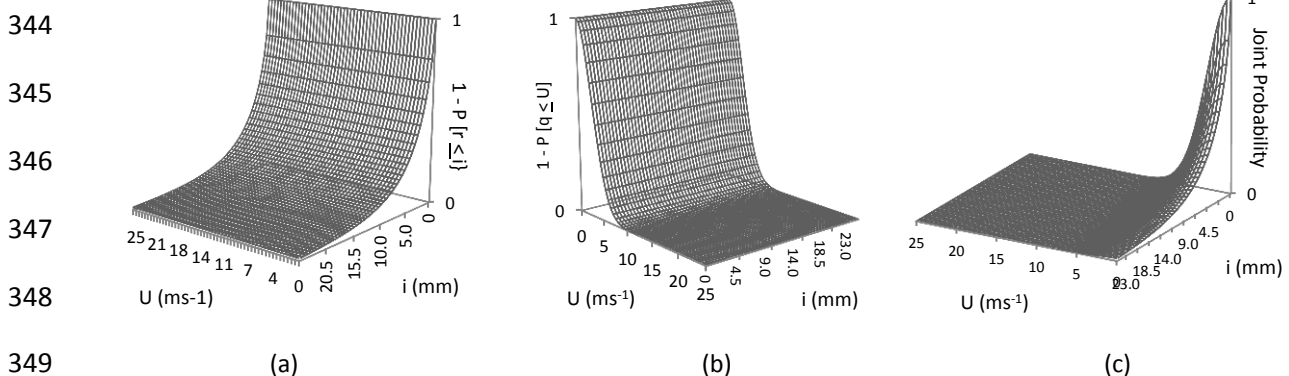
328 Fig. 9 shows that the increase of lodging is not linear with the variation of Cd . This might be due to
329 the fact that as the plant takes more load the mode of failure can switch from stem to root failure and
330 vice versa depending on the characteristics of the root. Note for instance that whereas about 95% of
331 the crop would have failed for when Cd equals 1.0 and U reaches 10 ms^{-1} only about half of it would
332 have done so when Cd equals 0.36 and for the same level of wind.

333 Finally, the probabilistic description for wind and rain at the locality of Cardington, given in section 3
334 was used to determine the probability associated to oat failure whilst subject to the combined effect of
335 wind and rain. Since wind and rain are considered to be uncorrelated¹ the probability of plant failure
336 associated to each pair $\{U, i\}$ is taken as the product of the probability associated to U_j and i_k being
337 exceeded, times the index N_{fail}/N_{plant} – see Eq. (9).

338
$$P[M_b > M_s || M_b > M_r] = (1 - P[r \leq i]) \cdot (1 - P[q \leq U]) \cdot \frac{N_{fail}}{N_{plant}} \quad (9)$$

339 where r, q are random variables representing rain and wind respectively. A description of the
340 probability that daily rain and hourly wind are exceeded together with the corresponding joint
341 probability are given in Fig. 10. The estimated probability of failure – see Eq. (9), for a range of wind
342 speeds occurring for daily rain of 2 mm is shown in Table 7.

343



¹ This is an assumption and is also the assumption in Baker et al. (2014). Although it can be argued that some correlation exists for stronger winds (Tsimplis, 1994), there is not enough evidence to assume there is correlation at medium or low wind levels.

350 Fig. 10. Probability of i and U being exceeded (a, b) together with their joint probability (c).

351

352 It can be seen in Fig. 10c that the combined action of i and U makes the crop failure more susceptible
353 to occur at relatively low levels of rain and wind. This is because the curves shown in Fig. 10 are
354 fairly flat at high values of i and U . Moreover, the region of higher joint probability of the pair $\{i, U\}$
355 being exceeded coincides with low frequency of failure shown in Fig. 7b. This translates into low
356 probability of failure for the oat crop as shown in Table 7 for a selected number of seasons and for $i =$
357 2 mm.

358

Table 7. Probability of failure of oat crop (%) for $i = 2$ mm

U ms ⁻¹	Rain Season			
	Jan	Apr	Jul	Oct
2	0.0	0.0	0.0	0.0
4	0.08	0.04	0.04	0.07
6	0.42	0.18	0.13	0.3
8	0.42	0.16	0.08	0.23
10	0.13	0.05	0.02	0.06
12	0.02	0.01	0.0	0.01
14	0.0	0.0	0.0	0.0
16	0.0	0.0	0.0	0.0
18	0.0	0.0	0.0	0.0
20	0.0	0.0	0.0	0.0

359

360 In Table 7 can be seen that the probability of failure varies with i and it tends to be higher early or late
361 during the year i.e. whilst wind loads tend to increase as shown in Fig. 4. Moreover through a more
362 general analysis it was observed that the highest probability of failure during January was estimated as
363 of 0.81%, occurring around the pair $\{i = 0.5 \text{ mm}, U = 7 \text{ ms}^{-1}\}$. This suggests that oat crops would have a
364 rather low probability of failure in any season. In the following section it is shown that wind can have
365 an important impact on lodging associated to other types of plants.

366 8. Crop failure characterising four types of plants

367 The analyses above were extended to three other plant types. These are wheat, barley, and oilseed
368 rape i.e. those which together with oat are reported as the most produced in the UK (Verissimo, 2015).

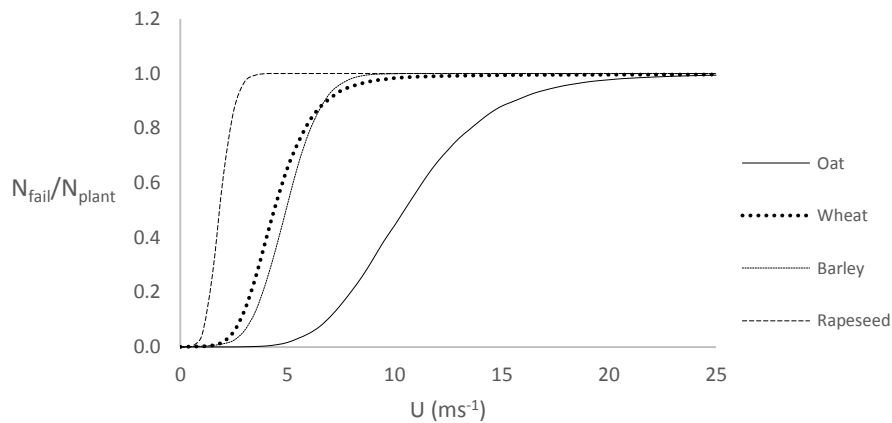
369 The parameters that characterise these cereal plants are provided in Table 8. Note that the parameter k_s
 370 refers to the root resistance defined by Eq. (7d) whilst m represents the characteristic mass of the
 371 plant's ear. For the sake of clarity, the oat parameters presented in Table 4 have also been included in
 372 Table 8.

373 Table 8. Parameters used to characterise target plant types

Plant Parameter	Plant Type – Mean Value				Plant Type – Standard Deviation			
	Oat ¹	Wheat ²	Barley ³	Rapeseed ¹	Oat ¹	Wheat ²	Barley ³	Rapeseed ¹
X (mm)	950	426	800	1520	150	34.08	65	200
A (mm ²)	10000	8000	9500	37000	3000	800	280	3000
d (mm)	6.6	3.35	5.32	11.1	1.0	0.402	0.85	2.0
n (Hz)	1.4	0.92	0.75	0.5	0.2	0.138	0.093	0.1
h (mm)	70	40	90	123	10	8.0	12.5	15
D (mm)	50	38	44	16.5	10	8.36	12.75	3.0
t (mm)	1.0	0.64	1.35	2.2	0.2	0.147	0.16	0.5
R (Nmm ⁻²)	30	30	27	25	5.0	9.9	2.8	5.5
m (Kg)	0.008 ³	0.006 ³	0.005	0.01 ⁴	-	-	-	-
k_s	0.43	0.43	0.58 ⁵	4.0 ¹	-	-	-	-
N	2.5	3.2	4.4	8.2	0.5	1.152	0.5	1.0

374 ¹ Baker et al (2014); ² Berry et al (2003); ³ Verissimo (2015); ⁴ Author's estimate based on Berry et al (2013); ⁵ Berry et al (2006)

375 In line with the analysis described above, plant databases conformed by 10,000 elements were subject
 376 to the combined action of wind and rain. Figure 11 shows the estimation of plant failure in terms of
 377 the index N_{fail}/N_{plants} , for all the groups. For the sake of simplicity only those results calculated for 2
 378 mm of rain are shown.



379

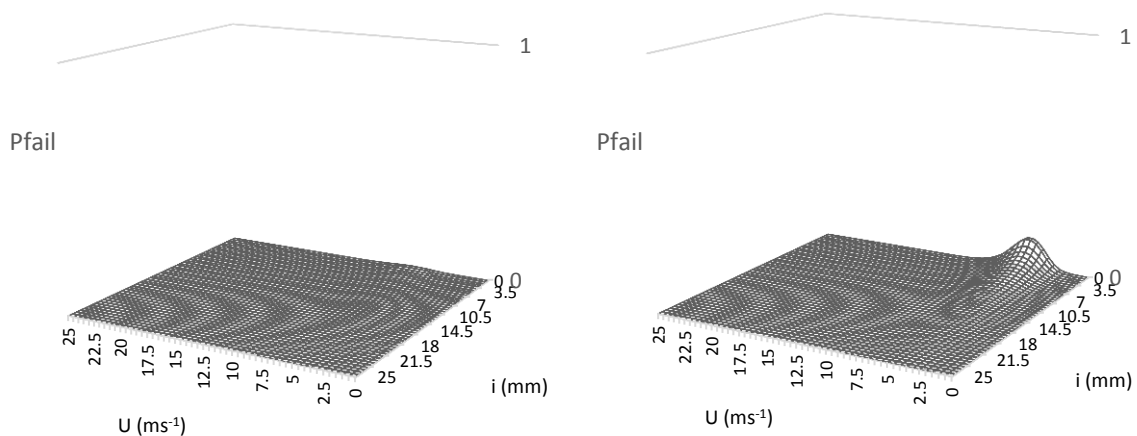
380

Fig. 11. Representation of plant's failure when $i = 2$ mm.

381

382 In Fig. 11 can be seen that rapeseed is the more susceptible to fail, opposite to oat which to an extent
383 could withstand wind speeds of 10 ms^{-1} and above. Wheat and barley have a similar behaviour with
384 slight differences below and above a wind speed of around 6.5 ms^{-1} – the point where their
385 performance seems to match. The results obtained also enable an average failure velocity to be
386 inferred. Let that threshold value be the velocity of wind at which $\sim 50\%$ of the crop fail. According to
387 this the mean failure velocity for the plant types analysed is of approximately 1.6 ms^{-1} , 4.5 ms^{-1} , 5 ms^{-1}
388 1 , and 10.5 ms^{-1} , for rapeseed, wheat, barley, and oat, respectively. Similarly the ultimate failure
389 velocity i.e. the one that would virtually cause total failure of the crop, is of 4.0 ms^{-1} , 8.5 ms^{-1} , 12 ms^{-1} ,
390 and 23 ms^{-1} for rapeseed, barley, wheat, and oat, respectively. Note that these reference velocities are
391 valid for a level of rain of 2 mm.

392 On the other hand, based on Eq. (9), the probability of plant's failure was calculated. As noted above
393 the shape of the joint probability distribution restricts the lodging domain in the direction of both
394 variables i and U . This can be observed in Fig. 12 which corresponds to the first month of the year –
395 the season identified as critical for lodging to occur.



396

397

398

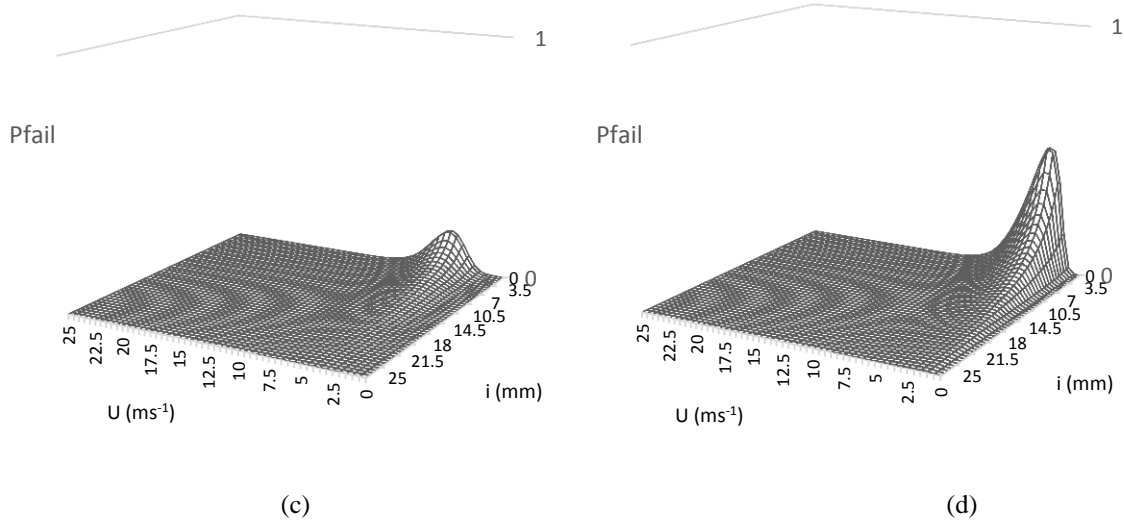


Fig. 12. Probability of failure of (a) oat, (b) barley, (c) wheat, and (d) rapeseed, during January.

399

400

401

402

403

404 The results presented in Fig. 12 confirm the low susceptibility of oat crops to fail. As discussed in the

405 previous section the highest probability associated to oat lodging is of 0.81%. The peak values

406 observed in Fig. 12 occur at low levels of rain – where according to Eq. (7c) and Fig. 6 lodging would

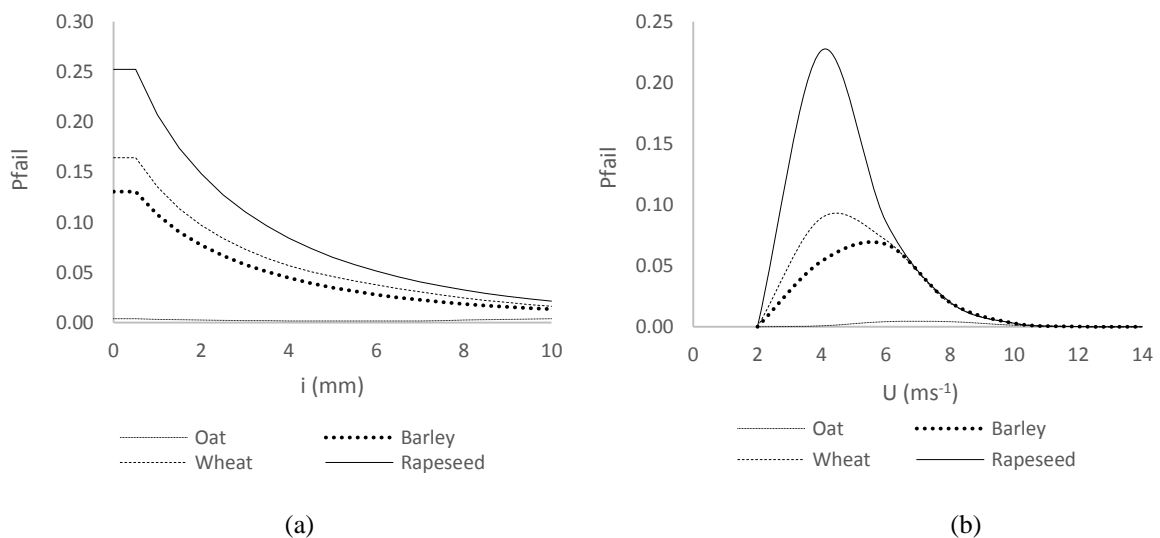
407 be controlled by stem resistance. Peak values in the curves shown in Fig. 12 are of 0.81% for oat

408 when $U = 7 \text{ ms}^{-1}$, 13% for barley with $U = 5.5 \text{ ms}^{-1}$, 17% for wheat with $U = 4.5 \text{ ms}^{-1}$, and 50% for

409 rapeseed when $U = 3 \text{ ms}^{-1}$.

410 For the sake of clarity the probability of failure derived from crop performances is illustrated in Fig.

411 13 by using reference values of (a) velocity $U = 5 \text{ ms}^{-1}$ and (b) rain $i = 2 \text{ mm}$.



412

413

414

415 Fig. 13. Probability of failure estimated for all plant types (a) with $U = 5 \text{ ms}^{-1}$ and (b) with $i = 2\text{mm}$.

416

417 In section 6 it was discussed how the plant's root strength increases as i decreases. This is also being
418 reflected in Fig. 13a where is shown that in region of low rain the probability of lodging to occur is
419 being controlled by stem resistance – see also Fig. 6. Fig. 13a also shows that at least for $U = 5 \text{ ms}^{-1}$,
420 wheat has more chances to fail than barley whilst both plant types would report ~50% less failure than
421 rapeseed but more than 100% of the failure that can be associated to oat. In Fig. 13b becomes evident
422 that each plant type responds differently when subject to the same level of rain. This is illustrated by
423 the relative position of the peak probability of failure. This figure also shows that the interval $2 \leq U \leq$
424 10 ms^{-1} is where lodging of any crop is susceptible (in a probabilistically sense) to occur. This is in
425 principle valid for a level of rain of 2 mm, however looking at Fig. 12 it seems that no much
426 difference would make to have levels of rain of up to about 10 mm.

427 9. Final Remarks

428 The paper has shown a method to estimate crop failure by using statistical descriptions of the climate
429 such as those provided by the UKCP09 Weather Generator together an existing theoretical model to
430 calculate the plant's response. The weather scenarios studied cover a horizon of 30 years. The data
431 predicts an increase of wind velocities of about 4.5% with respect to current conditions. The weather
432 predictions also suggest that the level of rain that is exceeded 50% of the time will range between 1.75
433 mm during April and 2.75 mm in November. That makes a yearly average of 2.25 mm i.e. slightly
434 above the current reference value of 2 mm. Regarding the crop responses, the study identifies oats as
435 the most resilient type of plant from the group whilst rapeseed appears to be the most susceptible to
436 fail. For example the failure velocity for 100% of the oat crop is estimated as of 23 ms^{-1} and it is of 4
437 ms^{-1} for rapeseed, for a level of rain that is exceeded 50% of the time. The prediction model also
438 indicates that the failure velocity will become constant after a threshold value of rain (that is exceeded
439 50% of the time) in the region of 7.5 mm i.e. stem failure would dominate the plant's failure after that
440 point. Finally, the proposed research methodology suggests three areas of development: (a) the

441 interaction of plants in motion and with the changes caused in the boundary layer during that process,
442 (b) the availability correlated wind and rain statistics, and (c) development of finite element models
443 that enable to observe the flow of stress and rate of deformation experienced by different segments of
444 plants at the time that allow quantifying lodging i.e. modelling large populations of plants at high
445 resolution.

446

447

448 **Appendix A: Steps to generate climate scenarios by using the UKCP09 Weather Generator**

449

450

1 Pathway

- i. UK probabilistic projections of climate change over land
- ii. UK probabilistic projections of climate change over marine regions
- iii. Weather generator simulator
- iv. Past and future multi-level ocean simulations for UK waters
- v. Projections of trend in storm surge for UK waters
- vi. Projections of sea level rise for UK waters

Option (iii)

456

457

2 Emission scenario

- i. Low
- ii. Medium
- iii. High

Option (ii)

3 Time period

- i. 2020s: 2010-2039
- ii. 2030s: 2020-2049
- iii. 2040s: 2030-2059
- iv. 2050s: 2040-2069
- v. 2060s: 2050-2079
- vi. 2070s: 2060-2089
- vii. 2080s: 2070-2099

Option (i)

460

4 Location

e.g. Rosemaud, Cardington (52.11 °N,
0.424 °W 83 m above MSL)

464

465

5 Sampling method

- i. All
- ii. Random sampling of model variants
- iii. Specific set of model variants
- iv. Particular sub-set of probabilities

Option (ii)

470

6 Configuring weather generator

- i. Daily
- ii. Hourly

Option (all)

472

473

7 Format output file

- i. Map
- ii. Raw data
- iii. Joint probability plot
- iv. Plume plot
- v. Return periods plot
- vi. Cumulative distribution function
- vii. Probability density function

Option (ii)
CSV file

477

478 **Appendix B: Equations to calculate U_2 from known environmental parameters**

479 $X = 0.408\Delta(R_n - G); Y = \gamma \frac{900}{T+273.16}; Z = e_a - e_d$ (B1)

480 $\Delta = 0.04145e^{0.060887T}$ (B2)

481 $\gamma = \frac{(c_p)_{air}P}{\lambda_v MW_{ratio}}$ (B3)

482 $e_a = 6.112 \exp\left(\frac{17.67T}{T+243.5}\right)$ (B4)

483 $R_n = R_{ns} - R_{nl}$ (B5)

484 $R_{ns} = (1 - D)R_s$ (B6)

485 $R_{nl} = s \left[\frac{T_{max,K^4} + T_{min,K^4}}{2} \right] (0.34 - 0.14\sqrt{e_d}) \left(1.35 \frac{R_s}{R_{so}} - 0.35 \right)$ (B7)

486 $R_s = k_{RS} \sqrt{T_{max} - T_{min}} R_a$ (B8)

487 $R_a = \frac{24 \cdot 60}{\pi} G_{sc} d_r [\omega_s \sin(\varphi) \sin(\delta) + \cos(\varphi) \cos(\delta) \sin(\omega_s)]$ (B9)

488 $R_{so} = (0.75 + 2 \times 10^{-5} Z_s) R_a$ (B10)

489 $\varphi = \frac{\pi}{180} \left(Lat_{deg} + \frac{Lat_{min}}{60} \right)$ (B11)

490 $d_r = 1 + 0.033 \cos\left(\frac{2\pi J}{365}\right)$ (B12)

491 $\delta = 0.409 \sin\left(\frac{2\pi J}{365} - 1.39\right)$ (B13)

492 $\omega_s = \arccos[-\tan(\varphi) \cdot \tan(\delta)]$ (B14)

493 where,

494 P : atmospheric pressure (kPa)

495 λ_v : latent heat of water vaporisation = 2.45 (MJ kg⁻¹)

496 c_p : specific heat of air at constant pressure (MJ kg⁻¹ °C⁻¹) = 1012 × 10⁻⁶

497 MW_{ratio} : ratio molecular weight of water vapour/dry air = 0.622

498 R_{ns} : shortwave net radiation (MJm⁻²day⁻¹)

499 R_{nl} : long wave net radiation (MJm⁻²day⁻¹)

500 D : albedo or canopy reflection coefficient = 0.23

- 501 s : Stefan-Boltzmann constant = 4.903×10^{-9} ($\text{MJK}^4 \text{m}^{-2} \text{day}^{-1}$)
- 502 T_{max} : maximum absolute temperature during the 24-hour period [$\text{K} = ^\circ\text{C} + 273.16$]
- 503 T_{min} : minimum absolute temperature during the 24-hour period [$\text{K} = ^\circ\text{C} + 273.16$]
- 504 e_d : actual vapour pressure (kPa)
- 505 R_s : solar or short wave radiation ($\text{MJK}^4 \text{m}^{-2} \text{day}^{-1}$)
- 506 R_{so} : clear-sky radiation ($\text{MJK}^4 \text{m}^{-2} \text{day}^{-1}$)
- 507 R_a : extra-terrestrial radiation ($\text{MJK}^4 \text{m}^{-2} \text{day}^{-1}$)
- 508 z_s : station elevation above the sea level
- 509 G_{sc} : solar constant = 0.082 ($\text{MJm}^{-2} \text{min}^{-1}$)
- 510 d_r : inverse relative distance Earth-Sun
- 511 ω_s : sunset hour angle (rad)
- 512 φ : latitude (rad)
- 513 δ : solar declination (rad)
- 514 J : day number within a year i.e. $1 \leq J \leq 365$
- 515
- 516

517 **References**

- 518 Allen M R, Smith M, Pereira L S, Perrier A, 1994. An update for the calculation of reference evapotranspiration. *ICID*
519 *Bulletin*, 43:35-92.
- 520 Baines G B K, 1972. Turbulence within a wheat crop. *Agricultural Meteorology*, 10:93-105.
- 521 Baker C J, 1995. The development of a theoretical model for the wind-throw of plants. *J Theoretical Biology*, 175:355-372.
- 522 Baker C J, Berry P M, Spink J H, Sylvester-Bradley R, Griffin J, Scott R K, et al, 1998. A method for the assessment of the
523 risk of wheat lodging. *J. Theoretical Biology*, 194:587-603.
- 524 Baker C J, Sterling M, Berry P, 2014. A generalised model of crop lodging. *J Theoretical Biology*, 363:1-12.
- 525 Berry P M, Sterling M, Baker C J, Spink J H, Sparkes D L, 2003. A calibrated model of wheat lodging compared with field
526 measurements. *Agricultural and Forrest Meteorology*, 119:167-180.
- 527 Berry P M, Sterling M, Mooney S J, 2006. Development of a model of lodging for barley. *J. Agronomy & Crop Science*,
528 192(2):151-158.
- 529 Berry P M, White C, Sterling M, Baker C, 2013. Develop a model of lodging in oilseed rape to enable integrated lodging
530 control to reduce PGR use. *CRD Project PS2146*, September.
- 531 Cionoco R M, 1972. A wind profile index for canopy flow. *Boundary Layer Meteorology*, 3(2):255-263.
- 532 Denmead O, Bradley E F, 1967. The collection and processing of field data. *John Wiley and Sons*, New York.
- 533 Dyrbye C, Hansen S, 1997, Wind loads on structures. *John Wiley and Sons*, New York.
- 534 Ekström M, Jones Pd, Fowler Hj, Lenderink G, Buishand Ta, Conway D, 2007. Regional climate model data used within the
535 SWURVE project 1: Projected changes in seasonal patterns and estimation of PET. *Hydrol Earth Syst Sci*, 11: 1069–83.
- 536 Eames M, Kershaw T, Coley D, 2011. On the creation of future probabilistic design weather years from UKCP09. *Building*
537 *Services, Engineering, Research, and Technology*, 32(2):127-142.
- 538 Finnigan J J, Mulheran P J, 1978. Modelling waiving crops in a wind tunnel. *Boundary Layer Meteorology*, 14:253-277.
- 539 Finnigan J, 2000. Turbulence in plant canopies. *Annu. Rev. Fluid Mech.* 32:519-571.
- 540 Kaimal J C, Finnigan J, 1994. Atmospheric boundary layer flows: their structure and measurement. *New York: Oxford*
541 *Univ. Press*, 289.
- 542 Langre E, 2008. Effect of wind on plants. *Annual Review of Fluid Mechanics*, 40: 141-168.
- 543 Liu H L, Roble R G, Taylor W R, Pendleton W R, 2001. Mesospheric planetary waves at northern hemisphere fall equinox.
544 *Geophysical Research Letters* 28(9):19031906.

545 Martinez-Vazquez P, Sterling M, 2011. Predicting wheat lodging at large scales. *Biosystems Engineering*, 109(4), 326-337.

546 Met Office, 2013. Virtual Met Mast report for meteorological research unit, Cardington. *Met Office*.

547 Jenkins G J, Murphy J M, Sexton D M, Lowe J A, Kilsby C G, 2009. UK Climate predictions: briefing report. *Met Office*

548 *Hadley Centre*, Exeter, UK.

549 Rodriguez M, Moulia B, De Lagrange E, 2009. Experimental investigation of a walnut tree multimodal dynamics. 7

550 *Euromech Solid Mechanics Conference*. Lisbon. 7-11 Sept.

551 Sellier, D, Fourcaud T, And Lac P, 2006. A finite element model for investigating effects of aerial architecture on tree

552 oscillations. *Tree Physiology* 26: 799 – 806.

553 Sterling M, Berry P M, Baker C J, Wade A, 2003. An experimental investigation of the lodging of wheat. *Agricultural and*

554 *Forrest Meteorology*, 119:149-165.

555 Saunderson S E T, Baker C J, England A, 1999. A dynamical model of the behaviour of Sitka Spruce in high winds. *J.*

556 *Theoretical Biology*, 2000:249-259.

557 Saunderson S E T, Baker C J, England A, 2000. A dynamic analysis of the wind throw of trees. *Forestry*, 73(3):225-237.

558 Tsimplis M N, 1994. The correlation of wind speed and rain. *Weather*. 49(4): 135-139.

559 Ventura F, Spano D, Duce P, Snyder R L, 1999. An evaluation of common evapotranspiration equations. *Irrig. Sci.* 18:163-

560 170.

561 Verissimo H, 2015. Quantification of cereal lodging at small and large scales. *MSc Thesis*. University of Birmingham, UK

562 Wright J L, 1965. Evaluating turbulent transfer aerodynamically within the microclimate of a cornfield. *PhD Thesis Cornell*

563 *University*, Ithaca New York.